Journal of Biomedical Optics 5(4), 375–382 (October 2000)

Design and characterization of a laser-based instrument with spectroscopic feedback control for treatment of vascular lesions: the ''Smart Scalpel''

Elizabeth L. Sebern
Colin J. H. Brenan
Ian W. Hunter
Massachusetts Institute of Technology
Department of Mechanical Engineering, Room 3-147
Cambridge, Massachusetts 02139

Abstract. To improve the effectiveness of microsurgical techniques, we are developing a semi-autonomous robotic surgical tool (called the ''Smart Scalpel'') as an alternate approach to treatment of vascular lesions. The device employs optical reflectance spectroscopy as part of a line scan imaging system to identify and selectively target blood vessels in a vascular lesion for thermal treatment with a focused laser beam. Our proof-of-concept reported here presents the design and construction of a prototype instrument, initial quantification of imaging system resolution and contrast, and preliminary verification of the imaging and targeting strategies with standard targets and live dermal tissue.
[S1083-3668(00)00804-2]

Keywords: vascular lesion; microsurgery; optical reflectance spectroscopy; robotic feedback control.

Paper 90033 received June 3, 1999; revised manuscript received June 20, 2000; accepted for publication July 7, 2000.

1 Introduction

Real-time, automated closed-loop feedback control is widespread throughout many engineering disciplines, but is virtually nonexistent in surgical instrumentation. An interesting potential application of feedback control is in the field of microsurgery. Many microsurgical procedures require a high degree of physical dexterity, accuracy, and control, which may degrade rapidly with physician fatigue. This problem could be partially alleviated through inclusion of low-level, automated decision making embedded in a microsurgical tool to aid in tissue location and removal.

Our general embodiment of this concept (Figure 1), a device we call the ''Smart Scalpel,'' noninvasively measures the physico–chemical properties (morphological, biochemical, mechanical, electrical, etc.) at points distributed within a volume of tissue and utilizes this information for continuous feedback control of the selective targeting and treatment of diseased or damaged tissues with a spatially localized energy source, leaving the surrounding healthy tissue intact.[1,2] A numerical model of tissue properties integrating expert physician knowledge is combined with real-time physico–chemical measurements and input from a human operator (physician) to accurately locate and identify the targeted tissue type. This automated imaging and targeting sequence is repeated until all the selected tissue has been treated.

Inclusion of automated, real-time feedback control in microsurgical instrumentation can potentially improve the accuracy and reliability of current microsurgical procedures by minimizing collateral damage to surrounding tissue and through inclusion of quantitative, on-line assessment of treatment efficacy. Potential patient benefits include increased comfort, shortened recovery times, and an overall decrease in the cost per procedure. Additionally, the computerized and robotic nature of the Smart Scalpel lends itself well to integration into a tele-operation system for remote surgery.

One potential application of this device is laser treatment of vascular lesions, particularly telangiectasias. Vascular lesions are currently treated by illuminating the blood vessels in the lesion at a wavelength coincident with an oxyhemoglobin absorption band (415, 540, 577, or 940 nm). Selective photothermolysis heats the blood relative to the surrounding tissue to a point at which necrosis occurs.[3] Telangiectasias are partially characterized as having a network of relatively large, widely spaced blood vessels, which makes this class of vascular lesion a likely candidate for treatment with an automated targeting and treatment system. In contrast, treatment of vascular lesions comprised of denser vessel networks, such as hemangiomas (port wine stain), with this approach may be less effective due to optical scattering in the epidermis that potentially degrades both image resolution and coupling of laser energy into the targeted vessels.[4]

Current laser treatment of telangiectasias involves tracing of individual vessels by hand with a focused visible light laser beam.[5–9] Blood vessels having diameters from 0.1 to 1 mm[5] have been treated in this way with laser fluence levels 90–200 kJ/m^2,[6,9,10] illumination spot diameters 1–7 mm,[9–11] and pulse durations 0.5–1.5 ms.[6,10] Multiple treatments are typically required for adequate clearing of the lesion (three treatments at 6 week intervals)[6] and cooling the epidermis, with a water-cooled sapphire tip[9] or ice or a hydrogel dressing[10,11] is often necessary. Accurate targeting and focused illumination of blood vessels could partially alleviate nonspecific heating of

The present address of Elizabeth L. Sebern is: Ethicon Endosurgery, 4545 Creek Road, ML 62, Cincinnati, OH 45242.
Address all correspondence to: Colin J. H. Brenan, MIT Department of Mechanical Engineering, 77 Massachusetts Avenue, Room 3-147, Cambridge, MA 02139. Tel: 617-253–0634; Fax: 617-252-1849; E-mail: cbrenan@mit.edu

1083-3668/2000/$15.00 © 2000 SPIE

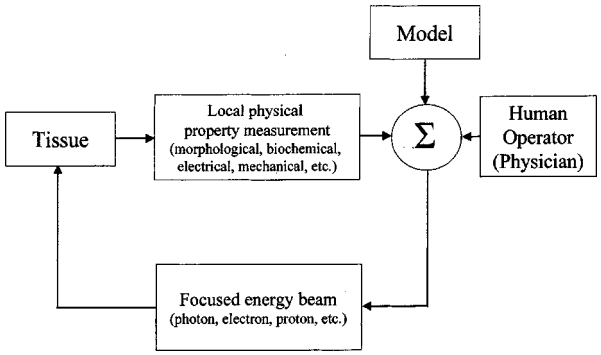

Fig. 1 Block diagram depicting a generalized automated system utilizing feedback derived from measurement of local tissue properties for automated closed-loop positioning control of a focused energy beam to locally modify tissue properties.

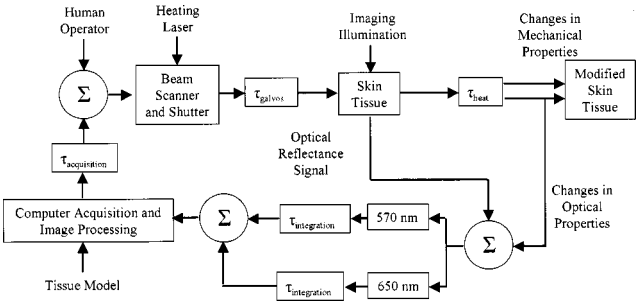

Fig. 2 Block diagram of system utilizing feedback based on measurement of local tissue properties for closed-loop control of the spatial positioning of a focused heating laser beam for potential treatment of vascular lesions.

the surrounding tissue leading to decreased collateral damage and an increased treatment efficacy.

As a first step toward evaluating this hypothesis, we describe here our development of a prototype system for closed loop, real-time identification, and targeting of blood vessels in dermal tissue. We begin with a system design overview summarizing the design criteria motivating our selection of a two-wavelength line scan imaging system for blood vessel detection and targeting. The imaging and closed-loop targeting characteristics of the prototype were found with standard target reticles and measurement of the axial and lateral modulation transfer function verified the resolution and field-of-view design criteria were suitable for vessel targeting in tissue. This performance was confirmed by application of the instrument to locating and targeting blood vessels in a mouse ear.

2 System Design

Efficient heating of a blood vessel volume demands there be little relative motion between the focused laser beam and vessel during image frame acquisition, processing, and laser targeting. Tremor is a major source of targeting error with a maximal displacement bandwidth of 10 Hz.[12] Thus to present a stabilized target to the focused heating laser beam, spectroscopic imagery of the area under treatment is continuously updated to provide the targeting information needed to compensate for tremor-induced relative motion between the laser beam focus and the blood vessel target. The imaging frame rate F_{frame} expressed as

$$F_{\text{frame}}=\frac{1}{N_{\text{lines}}\times(\tau_{\text{int}}+\tau_{\text{acq}}+\tau_{\text{galvo}})}, \tag{1}$$

needs to exceed 20 frames/s (equivalent to a feedback control bandwidth of 20 Hz) to prevent antialiasing of the targeting information. The number of image lines per frame is N_{lines}, τ_{int} is the photosensor integration time per image line, τ_{acq} is the time required to digitize and algorithmically process the photosensor signal and τ_{galvo} is the response time of the galvanometer-mounted mirror that steers the heating laser beam to the blood vessel target (Figure 2). The sum of these time constants is the overall system response time τ. For a nominal image size of 100 lines/frame and a frame rate of 20 frames/s, the maximum control loop time constant is at 0.5 ms/line; a reasonable design objective given judicious hardware selection and algorithm design can keep τ_{int} and τ_{acq} <0.1 ms/line and with resonant scanning systems, τ_{galvo} <1 ms/line.

The time to address and treat n blood vessel targets identified within the stabilized image field-of-view t_{treat} is t_{treat} $=n\tau_{\text{heat}}$, where τ_{heat} is the time required to heat a volume of blood vessel to a temperature T_c at which thermally induced necrosis occurs. Thermal conduction is the dominant mechanism of heat removal when a vessel is heated; thus, sufficient laser energy needs to be delivered to the vessel within a time comparable to the thermal relaxation time τ_r

$$\tau_r=\frac{d^2}{16\alpha} \tag{2}$$

to heat the blood to a temperature equal to or greater than T_c. Taking the blood vessel diameter to be d and a blood thermal diffusivity α estimated to be 1.15×10^{-7} m^2/s based on 70% water composition,[13] large diameter blood vessels characteristic of telangiectasia (400 μm) are estimated to have a characteristic thermal relaxation time of 84 ms.

We chose a line scan imaging scheme primarily for the ability to dynamically control the image size and to implement both feed-forward and feed-back control strategies as necessary elements in an optimal target selection strategy leading to minimization of t_{treat} for a given lesion (Figure 3). The number of vessel targets changes with imaged area; hence, t_{treat} can be optimized by simply increasing or decreasing the area scanned. A second optimization strategy implements feed-forward control through acquisition of target location in advance of laser scanning. This may be important with telangiectasias, where an effective treatment is to trace individual blood vessels from the smallest branches inward to the large supply vessels, routing blood flow away from the branches.[14]

A ready estimate of the laser power incident on the skin surface required to heat a volume of blood in a vessel to T_c during τ_r is possible if we assume the laser wavelength is coincident with an oxyhemoglobin absorption band and the focused laser beam diameter is comparable to a blood vessel diameter. Blood vessels in telangiectasias are located in the dermis 460 ± 170 μm below the surface and are typically

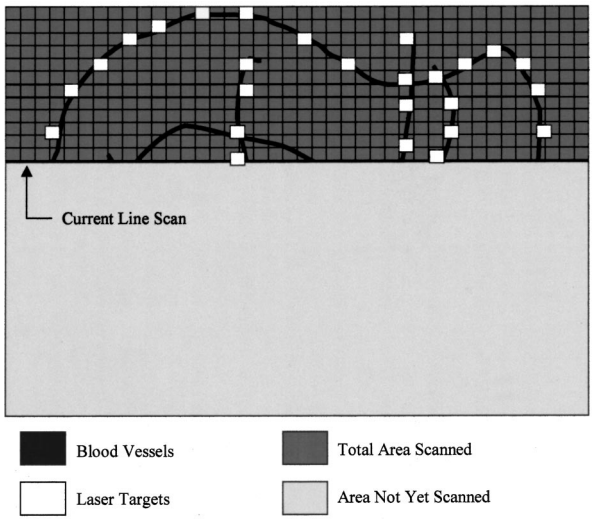

Fig. 3 Illustration showing coordination between line scan imaging for blood vessel identification and focused application of laser energy to selected points along the blood vessel.

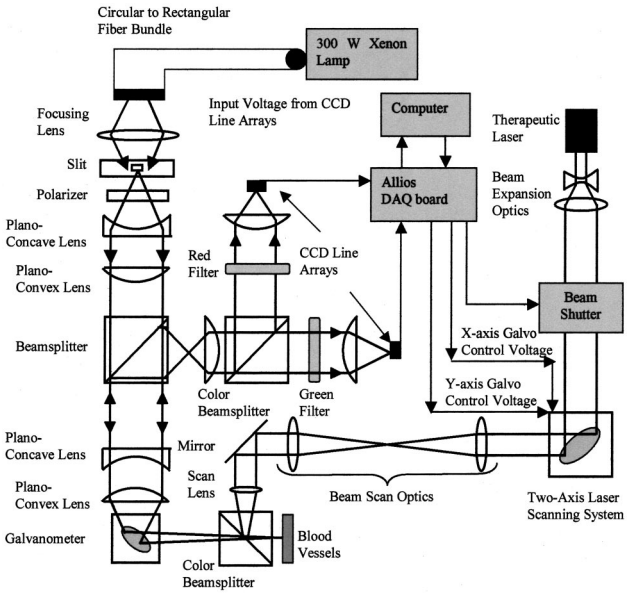

Fig. 4 Schematic of prototype spectroscopic line scan imaging and blood vessel targeting system design.

400 μm in diameter.[6] The laser power incident on the skin surface P_{inc} needed to raise the vessel temperature ΔT above ambient located a depth h below the surface is

$$P_{\text{inc}} = e^{h/\zeta} E/\tau_r = e^{h/\zeta} \frac{(\rho \pi r^2 d) c \Delta T}{\tau_r}, \tag{3}$$

where ρ is the density of blood [assumed to be similar to water ($\approx$1000 kg/m^3)], r is the radius of the laser spot ($\approx$250 μm), d is the blood vessel diameter ($\approx$400 μm), c is the specific heat of blood (assumed to be close to water, 4.2 kJ/kg/K), ΔT is the temperature rise required to coagulate the blood in the heated volume (approximately 30 K above ambient body temperature[14]) and ζ is the characteristic penetration depth of optical radiation in fair Caucasian skin at the illuminating wavelength ($\sim$390 μm @ 580 nm).[15,16] Setting h equal to 460 μm and evaluating Eq. (3) gives P_{inc} equal to 380 mW; a laser power achievable with many commercial lasers in current use for treatment of vascular lesions.

3 Methods

A prototype Smart Scalpel system is diagrammed in Figure 4. Light from a 300 W xenon lamp is passed through a fiber optic bundle having a circular-to-rectangular cross-section conversion (10 mm diameter to 0.8 mm$\times$9.7 mm rectangular cross section) to illuminate through a rectangular slit (50 μm$\times$6 mm) an optical system configured to generate a line of polarized white light on the skin. Light from the slit is collimated, passed through a beamsplitter cube, and focused onto the skin after reflection from a galvanometer-mounted mirror that scans the focused line of light across the skin's surface.

Light reflected and backscattered from the skin at each angular position of the scan mirror is descanned by the galvanometer mirror, reflected by the beamsplitter, separated into two wavelength bands using a color beamsplitter, and separately focused onto two linear charge coupled detector (CCD) photosensor arrays (1024 pixels, 25 μm$\times$2.5 mm pixels, 16 bit dynamic range). Light at wavelengths less than 630 nm is directed toward one array and is further spectrally filtered with a green bandpass filter [λ_{peak}=560 nm, full-width half-maximum (FWHM) 60 nm] to generate the oxyhemoglobin (blood) absorption signal. The green filter transmission bandwidth overlaps both 540 and 577 nm oxyhemoglobin absorption bands. Wavelengths longer than 630 nm pass through a red bandpass filter (λ_{peak}=650 nm, FWHM 50 nm) and generate the normalization (nonabsorption) signal. The overall magnification of the imaging system is 2.5, so that one pixel on the array corresponds to 10 μm on the skin surface. This resolution is sufficient to image 100 μm diam blood vessels, which will be the smallest targets to be resolved in telangiectasia. The scanned treatment area of 10 mm$\times$10 mm is a convenient interface between physician and patient and is similar to the area covered in current telangiectasia treatments.[8–10]

The photosensor outputs are recorded by the analog-to-digital converters (100 kS/s @ 16 bits/sample) of a custom-built data acquisition board (Allios[17]) on a PCI bus resident in a Pentium II PC and controlled by a program written in C. As each line image is recorded, one channel of the Allios board 18 bit digital-to-analog (D/A) converters is used to rotate the scan mirror to its next position. As each line image is read, a ratio image is computed and a threshold is set to determine the blood vessel locations. Processing of the ratio image to identify blood vessels is, at present, algorithmically straightforward. A histogram analysis of the ratio image sets a binary threshold in which all pixels below the threshold value (corresponding to high absorption) are identified as blood vessels. The vessel position in the imaging field of view is calculated and converted to target coordinates for the two-axis laser scanning system. The system acquires lines until the maximum number of targets that can be treated within the period of tremor has been identified. The coordinates of the targeted vessels are sent via two different D/A channels to two galva-

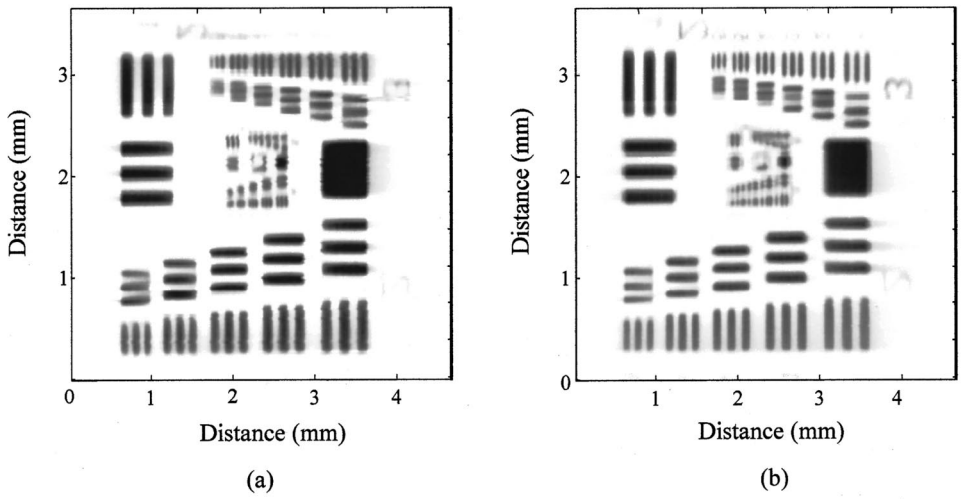

Fig. 5 Spectroscopic images of standard reticle to quantify lateral and axial imaging system resolution: (a) 560 nm and (b) 650 nm.

nometers (General Scanning) to direct the heating laser beam onto blood vessels identified and selected within the field of view. A fourth D/A channel controls an electro-optic beam modulator (Conoptics, Model 380) that blocks the heating laser beam to prevent heating of tissue during transit between targeted blood vessels.

4 Results

4.1 Modulation Transfer Function

To quantify the lateral and axial resolution of the imaging system, a standard test pattern of horizontal and vertical bars of known dimensions (Heidenhain), containing spatial frequencies from 0.25 to 228 mm^{-1} was imaged (Figure 5) within a 4 mm×6 mm field of view. The integration time per line was 40 ms resulting in a total of 8 s to acquire a 200 line×1024 pixel/line image.

The modulation transfer function (MTF) computed from this image quantifies the lateral spatial resolution of the imaging system. MTFs for the horizontal and vertical lines of the 560 nm (green) and 650 nm (red) channels of the in-focus target plotted in Figure 6 indicate the optical system is a low-pass spatial filter with a 50% attenuation bandwidth (MTF =0.5) of 10–12 mm^{-1} horizontally and 20–25 mm^{-1} vertically. This corresponds to a horizontal lateral resolution of 80–100 μm and a lateral resolution in the vertical direction of 40–50 μm. Horizontal lines are parallel to the line scan and vertical lines are perpendicular to the line scan. Similar results are observed for both the red and green channels. This is important since the ratio of these two signals is used to distinguish blood vessels from the surrounding tissue.

4.2 Depth of Focus and Field Flatness

Degradation in image contrast as a function of lateral and axial position relative to the focal plane was determined through measurement of the contrast of one spatial frequency (i.e., one point on the MTF) as a function of lateral and axial offsets from the in-focus position. In the case of the lateral offsets, contrast measurements were made for lateral offsets both perpendicular and parallel to the line scan axis. Figure 7 plots the contrast at one spatial frequency (8 mm^{-1} or 125 μm

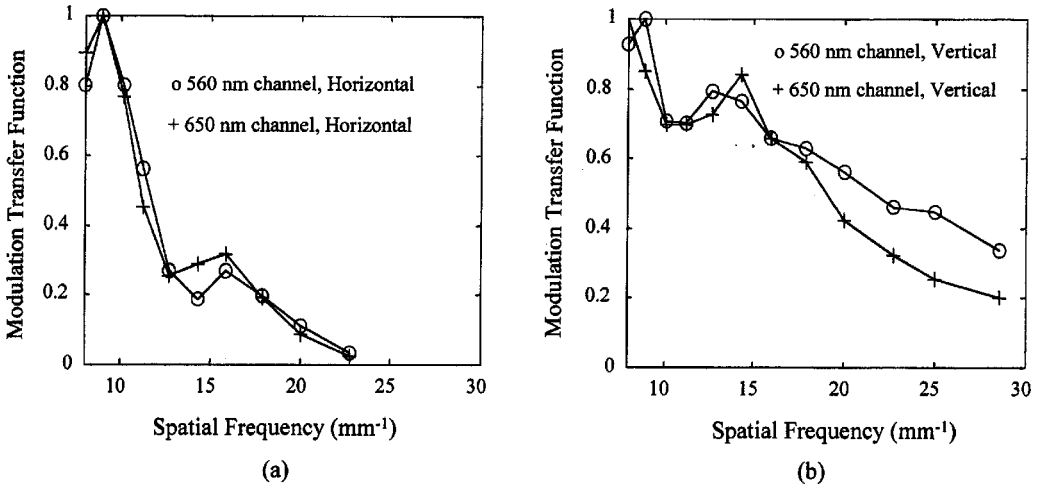

Fig. 6 Modulation transfer function for horizontal (a) and vertical (b) lines for 560 and 650 nm spectral channels.

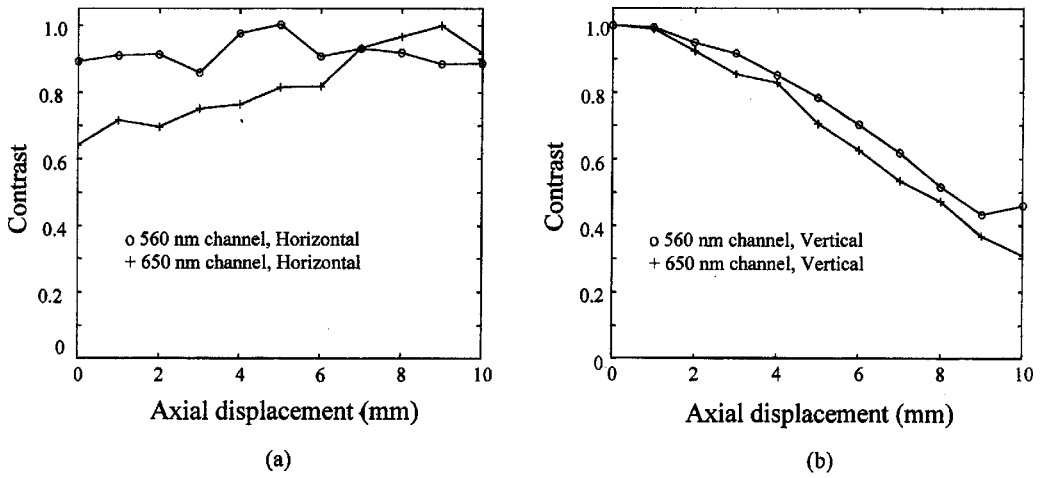

Fig. 7 Image contrast at 8 mm^{-1} vs axial position for horizontal (a) and vertical (b) lines.

spaced bars) as a function of axial position from the in-focus position ($z = 0$ mm). Each plotted contrast measurement is normalized with respect to in-focus contrast. Like the MTF versus spatial frequency measurements, contrast measurements for each spectral channel show similar trends. Based on the 50% attenuation criterion, the depth of focus is 8 mm for the vertical lines and greater than 10 mm for the horizontal lines.

Contrast parallel (x) and perpendicular (y) to the line scan direction is plotted in Figure 8 for each spectral channel at the 8 mm^{-1} spatial frequency. Contrast measurements in the x direction were made by moving the reticle parallel to the line scan across the imaging field, and measuring changes in the modulation amplitude with displacement. Zero lateral displacement is where the 125 μm bars are in the center of the imaging field. Applying the 50% attenuation criterion shows the extent of the field flatness to be 5 mm for the vertical lines and 6 mm for the horizontal lines. As with the axial displacement measurements, the vertical line modulation is more sensitive to position than was the horizontal line modulation. Similar results are observed for both spectral channels. Contrast measurements in the y direction was generated by measurement of the modulation amplitude of the 125 μm horizontal and vertical lines as a function of y position (Figure 9), with zero displacement where the bars are in the middle of the imaging field. Similar to the x-displacement data, the imaging field is flat across 3 mm for the horizontal bars and 4 mm for the vertical bars for each spectral channel.

4.3 Two-wavelength Imaging of Blood

To demonstrate the image acquisition and analysis sequence leading to blood vessel detection and targeting, we applied our system for two-wavelength imaging to distinguish fresh human whole blood from black ink in a test pattern on white paper (Figure 10). The ink was measured to have similar absorption coefficients at 560 and 650 nm. Images of the blood/ink test pattern were simultaneously acquired at 560 and 650 nm within 5 min of blood extraction and application to ensure the sample was representative of human oxyhemoglobin *in vivo*. The first image [Figure 10(a)] is from the green (560 nm) channel, which detects absorption of both blood and ink. Figure 10(b) is the red (650 nm) channel image, which shows only the black ink absorbance. The ratio image [Figure 10(c)]

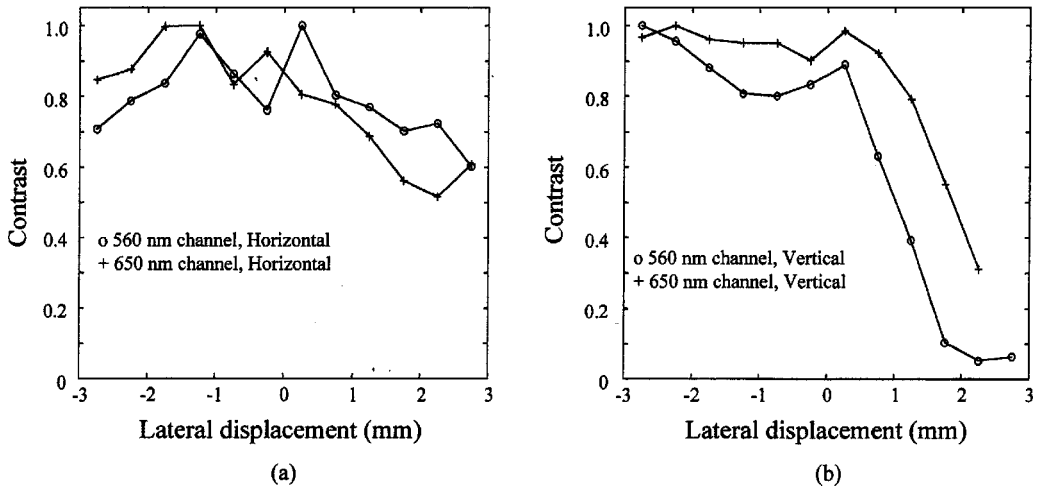

Fig. 8 Image contrast at 8 mm^{-1} of horizontal (a) and vertical (b) lines for lateral displacement parallel to line scan direction (x direction).

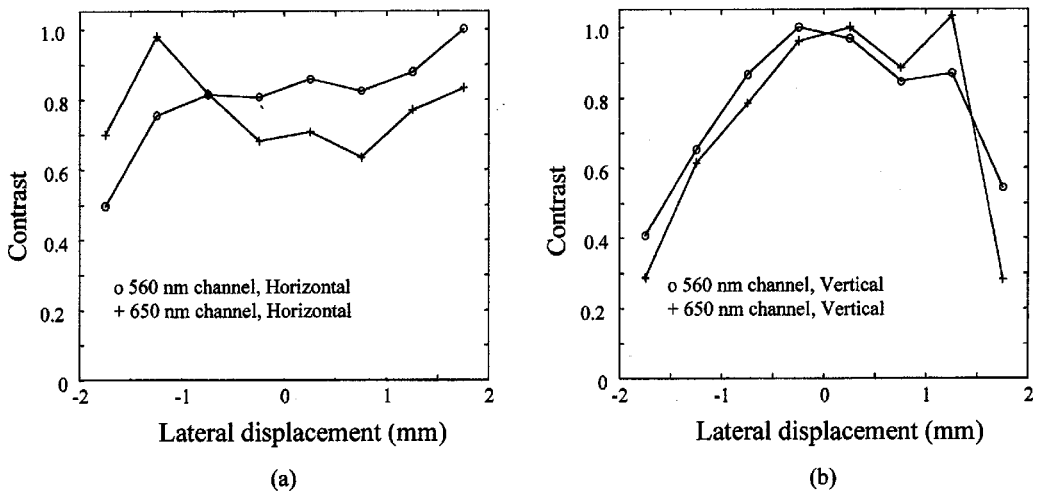

Fig. 9 Image contrast at 8 mm^{-1} of horizontal (a) and vertical (b) lines for lateral displacement perpendicular to line scan direction (*y* direction).

increases blood image signal-to-noise ratio (S/N) from 1.6 to 36, respectively. The S/N is defined as the ratio of the blood vessel modulation to the standard deviation of the background signal. Inspection of the image histogram [Figure 10(d)] suggested a threshold cutoff of 0.95 to generate the binary image [Figure 10(e)], where the black pixel positions are the target coordinates for input to the laser-scanning subsystem.

4.4 Closed-loop Control with Spectroscopic Feedback

Closed-loop imaging and laser targeting was tested with the bar reticle. After simultaneous acquisition of two spectral 50 line images of the reticle [Figure 11(a)], each image is normalized with respect to a uniformly reflecting target (mirror),

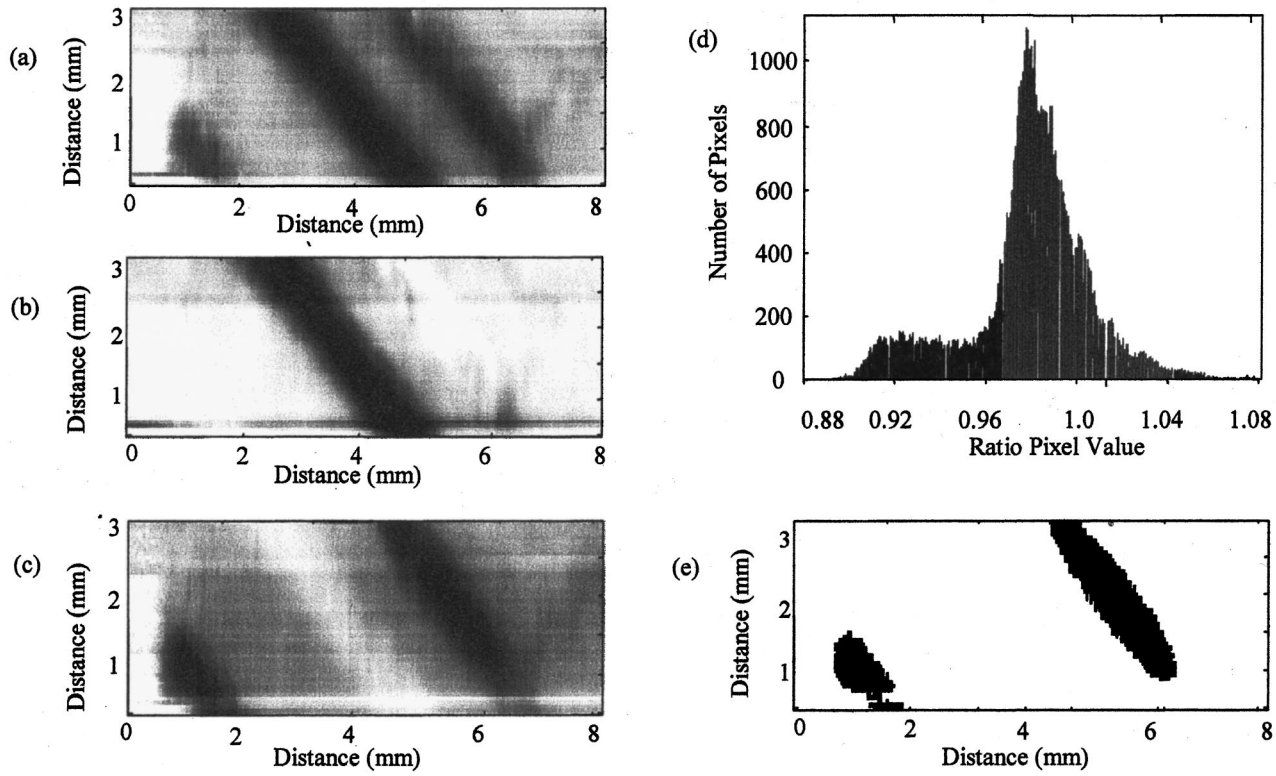

Fig. 10 Steps to distinguish blood from black ink deposited on white paper. (a) 560 nm channel image, which shows absorbance of blood and ink. (b) 650 nm channel shows only ink absorption. (c) Ratio image increases blood image contrast and suppresses ink signal. (d) Ratio image histogram used to generate the binary threshold image (e) used in laser targeting.

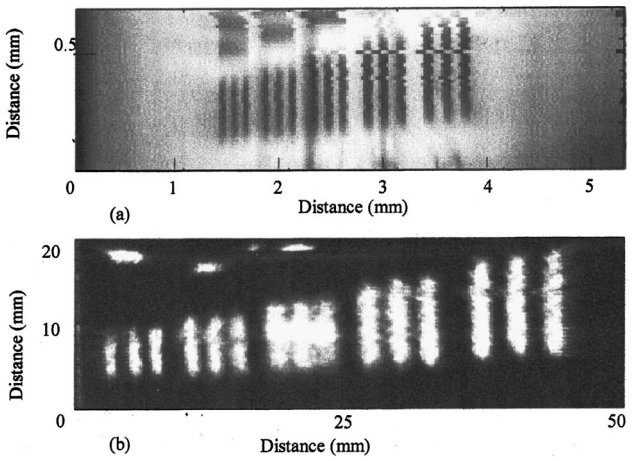

Fig. 11 Verification of laser scanning system using a test reticle image from the 560 nm channel (a). Pattern of light replicated by laser scanning system (b) from binary threshold image (threshold=0.8).

the ratio image is computed, and a threshold applied (0.8 threshold level) to generate a binary image from which the target (bar) coordinates are computed. A low power HeNe laser beam is raster scanned across a two-dimensional field and the shutter, while normally closed, is opened when the laser beam position coincides with a bar coordinate. A photograph of the resultant illumination pattern with a slow-scan CCD camera (4 s integration time) shows the reticle image is readily produced with high accuracy [Figure 11(b)]. Continuous image acquisition and laser targeting enabled lateral displacements of the reticle to be tracked within the control loop bandwidth of 0.2 Hz.

4.5 Blood Vessel Imaging in Live Tissue

As a proof-of-concept demonstration of the imaging and targeting capabilities of our prototype device, we analyzed the ear of a sedated albino mouse (70 gm) (Figure 12). The smaller reflectance of mouse dermis compared with the mirror reticle required several minor system modifications to increase the reflected optical signal. The slit width was increased from 50 to 500 μm to increase the illumination intensity, while decreasing somewhat the lateral resolution parallel to the line illumination, and the photosensor integration time was increased from 40 ms to 1 s to increase the recorded optical signal. The mouse rested comfortably in a custom-made holder and one ear was pressed gently between a glass slide and a cover slip to establish a flat imaging surface. The mouse and holder were mounted on a three-axis translation stage and the mouse was positioned to bring the ear into focus.

Figure 12 shows the series of operations used to generate a binary image of blood vessels in the mouse's ear. After simultaneous acquisition of two spectral images [580 and 650 nm, Figures 12(a) and 12(b), respectively] the ratio image is computed, median filtered, and background corrected [Figure 12(c)]. A line plot [Figure 12(d)] at the 4 mm vertical position shows at least two blood vessels (marked by arrows) and Figure 12(e) is a histogram of the ratio image. From these measurements, a 0.82 threshold level was selected and applied to generate the binary blood vessel image of Figure 12(f). Note the two vessels detected in Figure 12(d) are clearly marked in the threshold image.

5 Discussion

Our original design specifications for the Smart Scalpel prototype were motivated by the requirements inherent to auto-

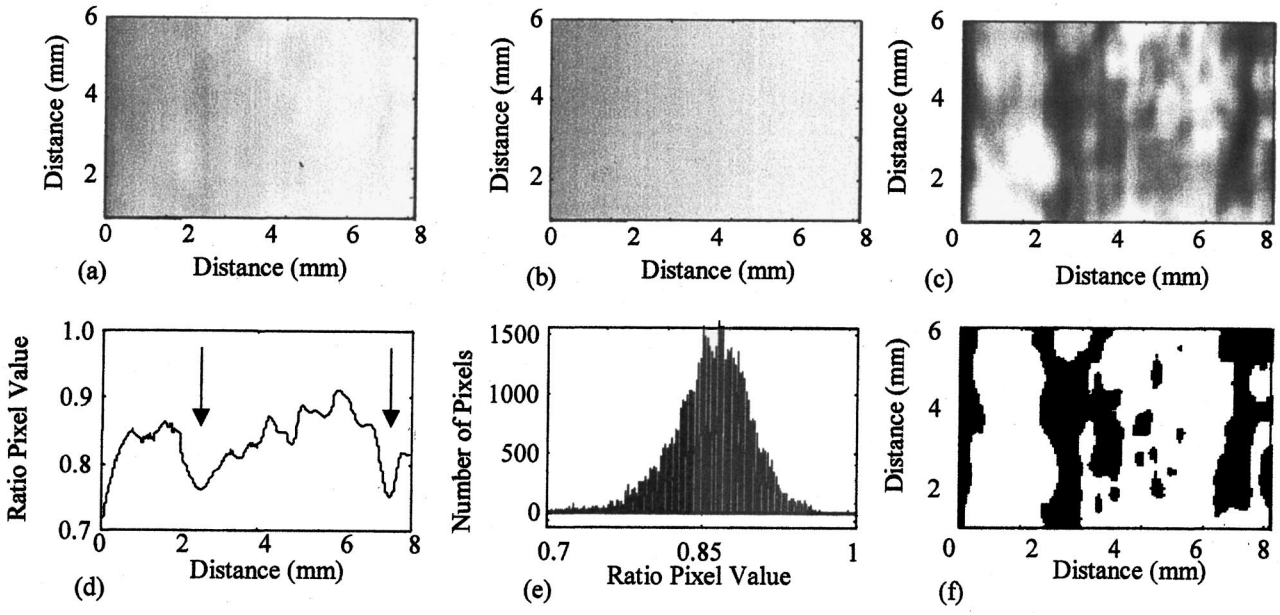

Fig. 12 Blood vessel images from 560 nm (a) and 650 nm (b) spectral channels. Ratio image (c) with median filtering correction for nonuniform illumination. Line plot of 4 mm vertical displacement (d) and image histogram (e) used to generate binary image (threshold=0.82) (f) of blood vessel targets.

mation of laser-based microsurgical procedures for treatment of different classes of vascular lesions having low spatial density of blood vessels. Accordingly our target design specifications included: (1) an image resolution <50 μm within a 10 mm$\times$10 mm treatment area, and (2) control loop bandwidth >10 Hz to compensate for tremor-induced relative motion between the blood vessel targets and treatment laser. With our prototype device, we achieved better than 50 μm vertical resolution and 100 μm horizontal resolution within a 4 mm$\times$6 mm treatment area. We measured the depth of focus to be 8 mm for vertical targets and greater than 10 mm for horizontal targets. Our optical system resolution is therefore suitable for detection of 50–100 μm sized blood vessels in the skin but in a smaller image field than originally specified. The line scan imaging system approach can be readily adapted to accommodate larger area images for treatment of vascular conditions such as telangiectasia where the vessel are distributed as a sparse vessel network within the dermis.

We demonstrated closed-loop tracking of targets identified from spectroscopic imaging feedback but with a bandwidth limited by delays inherent to the current system design ($\tau_{\mathrm{acq}}, \tau_{\mathrm{galvos}}$) and those associated with the optical and thermal properties of the skin ($\tau_{\mathrm{int}}, \tau_{\mathrm{heat}}$). With the mirror reticle, the instrument successfully tracked under closed-loop feedback control the motion of 100 μm spaced bars on a test pattern and replicated the imaged region with a scanned laser beam. Delays inherent to our data acquisition (DAQ) board and the galvanometer settling time limited the loop control bandwidth to 0.2 Hz. We anticipate an improvement by at least $\times$200 (40 Hz) with a faster DAQ board (10^6 samples/s) and galvanometers with shorter settling times (1 ms).

Low reflectivity of the mouse ear necessitated a higher illumination intensity and longer signal integration times to generate a signal sufficient for analysis leading to blood vessel identification. Consequently, the loop response time was too long and the image resolution degraded because of the requirement for a larger illumination slit width (500 μm vs 50 μm). One approach to increase illumination intensity without sacrificing spatial resolution or image acquisition times are high brightness optical sources in the two spectral bands of interest (580 and 650 nm). Possible candidates for illumination within the oxyhemoglobin absorption band (530–580 nm) include a frequency-doubled Nd:YAG laser (532 nm), a 543.8 nm HeNe laser, a dye laser, or sodium arc lamp. Candidate sources at the normalization wavelength ($>$600 nm) include a 632.8 nm HeNe laser or a visible/infrared laser diode.

Further increases in loop bandwidth can be achieved through more sophisticated target selection strategy that accommodates the intrinsic thermal relaxation time of the blood vessels. The current two-dimensional raster scan strategy is suboptimal because the entire imaged region is scanned. Through feed-forward control employing pattern recognition in advance of laser targeting, the laser need only trace the blood vessels identified, thereby considerably reducing the laser treatment time.

Acknowledgments

This work was supported by the MIT Lincoln Laboratory Advanced Concepts Committee and the MIT Home Automation and Health Care Consortium. We wish to thank Dr. Rox Anderson of the Wellman Laboratories of Photomedicine at the Massachusetts General Hospital for providing valuable clinical advice.

References

1. E. L. Sebern, C. J. H. Brenan, R. R. Anderson, and I. W. Hunter, ''Laser treatment of nevus flammus (port wine stain) with spectroscopic feedback: 'The Smart Scalpel,' '' *Proc. SPIE* **3590**, 32–42 (1999).
2. E. L. Sebern, C. J. H. Brenan, R. R. Anderson, and I. W. Hunter, ''Tissue modification with feedback: the 'Smart Scalpel,' '' *Proc. SPIE* **3519**, 62–69 (1998).
3. R. R. Anderson and J. A. Parrish, ''Selective photothermolysis: precise microsurgery by selective absorption of pulsed radiation,'' *Science* **220**, 524–527 (1983).
4. M. Keijzer, J. W. Pickering, and M. J. Van Gemert, ''Laser beam diameter for port wine stain treatment,'' *Lasers Surg. Med.* **11**(6), 601–605 (1991).
5. D. Reichert, ''Evaluation of the long-pulse dye laser for the treatment of leg telangiectasias,'' *Dermatol. Surg.* **24**(7), 737–740 (1998).
6. E. F. Bernstein, J. Lee, J. Lowery, D. B. Brown, R. Geronemus, G. Lask, and J. Hsia, ''Treatment of spider veins with the 595 nm pulsed-dye laser,'' *J. Am. Acad. Dermatol.* **39**(1), 746–750 (1998).
7. R. A. Neumann, H. Leonhartsberger, K. Bohler-Sommeregger, R. Knobler, E. M. Kokoschka, and H. Honigsmann, ''Results and tissue healing after copper-vapour laser (at 578 nm) treatment of port wine stains and facial telangiectasias,'' *Br. J. Dermatol.* **128**(3), 306–312 (1993).
8. E. Gonzalez, R. W. Gange, and K. Momtaz, ''Treatment of telangiectases and other benign vascular lesions with the 577 nm pulsed dye laser,'' *J. Am. Acad. Dermatol.* **27**(1), 220–226 (1992).
9. R. M. Adrian and Tanghetti, ''Long pulse 532 nm laser treatment of facial telangiectasia,'' *Dermatol. Surg.* **24**(1), 71–74 (1998).
10. U. Hohenleutner, T. Walther, M. Wenig, W. Baumler, and M. Landthaler, ''Leg telangiectasia treatment with a 1.5 ms pulsed dye laser, ice cube cooling of the skin and 595 vs 600 nm: preliminary results,'' *Lasers Surg. Med.* **23**(2), 72–8 (1998).
11. C. Chess and Q. Chess, ''Cool laser optics treatment of large telangiectasia of the lower extremities,'' *J. Dermatol. Surg. Oncol.* **19**(1), 74–178 (1993).
12. A. R. J. Elble and W. C. Koller, *Tremor*, The Johns Hopkins University Press, Baltimore, MD (1979).
13. A. L. McKenzie, ''Physics of thermal processes in laser-tissue interactions,'' *Phys. Med. Biol.* **35**(9), 1175–1209 (1990).
14. W. D. Tope (personal communication).
15. S. L. Jacques and S. A. Prahl, ''Modeling optical and thermal distributions in tissue during laser irradiation,'' *Lasers Surg. Med.* **6**, 494–503 (1987).
16. R. Rox Anderson and J. A. Parrish, ''The Optics of Human Skin,'' *J. Invest. Dermatol.* **77**, 13–19 (1981).
17. Electronic mail: http://biorobotics.mit.edu/home.html